Unified treatment of field-induced and intrinsic nonadiabatic transitions with a generalized Floquet Hamiltonian method

Kota Hanasaki* and Kazuo Takatsuka†

Department of Basic Science, The University of Tokyo, Komaba, 153-8902 Tokyo, Japan

(Received 14 December 2012; revised manuscript received 26 October 2013; published 25 November 2013)

We propose a generalized Floquet Hamiltonian method that is applicable to laser-induced molecular dynamics including nonperiodicity arising from time dependence of laser parameters and nuclear kinematic effects. Effects from these two types of nonperiodicity are formulated as generalized nonadiabatic transitions and treated in a unified manner. In this unified treatment, the field-induced dynamics of a molecule is mapped onto an effective nonadiabatic dynamics. An analog of the gradient approximation to the field-free nonadiabatic dynamics thus naturally follows and the relevant validity conditions are also formulated. Full-quantum-type numerical implementation of this method is applied first to the field-induced dynamics of H_2^+/D_2^+ within a two-state model and second to that of LiF based on the *ab initio* potential-energy surfaces. With the H_2^+/D_2^+ calculations, we confirm the validity of our formalism by reproducing the previously reported dissociation probabilities, which represent the phenomena of bond softening and bond hardening, including the "inverse bond-hardening effect" that has been identified in the present study. In the calculations of LiF, we realize full generalized *ab initio* Floquet analysis including the intrinsic nuclear derivative coupling. The effects of nuclear derivative couplings are assessed by directly comparing the calculations with and without the couplings. The present method, giving a simple and clear view of field-induced and kinematically induced nonadiabatic transitions, appears to be promising for the study of *ab initio* laser-induced dynamics of a system with nuclear derivative couplings.

DOI: 10.1103/PhysRevA.88.053426 PACS number(s): 33.80.Gj, 33.80.Wz, 42.50.Hz

I. INTRODUCTION

Laser-induced dynamics of molecules [1–3] has been a subject of intense research [4–6], reflecting its importance in understanding the nature of chemical bond formation and as a promising means for applications such as wave-packet engineering for chemical reaction control [7]. Recent developments in experimental techniques have achieved, for example, control over laser pulses with subfemtosecond resolution, enabling real-time observation of electronic dynamics in molecules [8–10]. Theoretical studies in this respect, on the other hand, still suffers from difficulties due to the nonperturbative nature of photon-molecule interactions, and indeed accurate calculations of laser-induced electron dynamics in a molecule are still a hard task even for diatoms or triatoms [11–15]. Since the studies of chemical reactions in the laser field [7,9] necessarily involves the dynamics of nuclei, full quantum-mechanical treatment of entire electron-nucleus dynamics, in particular, are prohibitively difficult except for the simplest molecules such as H_2^+ [16,17].

However, a part of the difficulties can be circumvented if one can approximate the nuclear dynamics by a quasiclassical method on effective potential-energy surfaces (PESs), just in analogy to field-free chemical dynamics [18–22]. In this respect the field-induced PES [23,24], which is obtained from the Floquet formalism [23–26], has been known as a corresponding notion of the field-free PES. In fact, the quasiclassical approximation of nuclear dynamics on the field-induced PES has been applied [27–29] to successfully describe the field-induced dynamics. Most notably, two fundamental mechanisms, the bond-softening [30–32] and the bond-hardening [29,33], have been clearly explained in terms of quasiclassical dynamics. However, the validity of the Floquet-based analysis is ambiguous when the exact periodicity (of the electronic Hamiltonian) is broken due to the nonperiodicity of the laser field and/or nuclear kinematic effects. Therefore the validity and its associated conditions should be theoretically established for the Floquet method to be safely applied to such aperiodic cases.

Another crucial effect to be considered in nuclear dynamics of molecules is intrinsic nonadiabatic transitions due to the nuclear derivative (kinematic) couplings. It is then expected that the interplay of field-induced deformation of PESs and the intrinsic nonadiabatic effects should lead to richer variety of dynamics, which is indeed realized as the dynamical Stark control in Ref. [1]. Inclusion of nuclear nonadiabatic effects in the Floquet analysis is therefore critical for the study of field-induced nonadiabatic dynamics. Both the nuclear kinematic effects and nonstationary laser fields introduce nonperiodicity in the electronic Hamiltonian, thereby breaking the stationarity of electronic Floquet states. Ho and Chu are the first who incorporated those nonstationarities of the Floquet states as generalized nonadiabatic transitions among them [34].

In order to make the theoretical ground of the Ho and Chu formalism more robust and widen the applicability range, we here restructure (reconstruct) the generalized Floquet Hamilton method by means of the two-time formalism of Pesikin and Moiseyev [35] [or what theses authors call (t,t') formalism] with appropriate modifications. With this generalized Floquet Hamiltonian method we treat electron-nucleus coupled chemical reaction dynamics under nonstationary laser fields controlled with time-dependent parameters. We also develop a numerical algorithm that enables unified and simultaneous calculations of all those kinds of nonadiabatic transitions.

*hanasaki@mns2.c.u-tokyo.ac.jp
†kaztak@mns2.c.u-tokyo.ac.jp

The theory thus implemented is applied to field-induced bond dynamics mainly to see how it works. We first calculate $H_2{}^+$ and its isotope $D_2{}^+$, using a modeled Hamiltonian without nuclear derivative couplings, to verify the present formalism. We will also examine whether this approach can provide clearer insights into the underlying mechanisms such as bond softening [30–32] and bond hardening [29,33]. We next treat a problem in which the intrinsic nuclear derivative couplings are explicitly involved. We are particularly interested in such systems where the nuclear kinematic effects play an essential role in a dissociation process. Such a system can be found, for example, in typical ionic bound diatomics, such as LiF, in which the lowest ionic and covalent PESs have an avoided crossing. We calculate *ab initio* PESs and matrix elements of LiF to perform dynamical calculations with all nonadiabatic effects fully taken into account. These results all show in the end that the present theory is promising as a general method for unified treatment of field-induced and intrinsic nonadiabatic transitions.

The organization of this paper is as follows; We first formulate the theory and method in Sec. II. Numerical calculations of $H_2{}^+/D_2{}^+$ and LiF are then discussed in Secs. III and IV, respectively. The paper concludes in Sec. V.

II. EXTENDED FLOQUET ANALYSIS

In this section, we formulate a generalized Floquet Hamiltonian method with use of two timelike variables, originally developed by Peskin and Moiseyev [35].

A. Two-time formalism of quantum dynamics

Let us begin with the time-dependent Schrödinger equation

$$i\hbar\frac{\partial}{\partial t}|\psi_t\rangle = H_t|\psi_t\rangle, \tag{1}$$

where $|\psi_t\rangle$ is the state vector of the system. Up to this point, no restriction is imposed on the time dependence of the Hamiltonian H_t. The state vector $|\psi_t\rangle$ is then extended to a function of two time variables $|\widetilde{\psi}_{t,s}\rangle$, which is related to the original or the physical state, by

$$|\widetilde{\psi}_{t,s}\rangle|_{t=s} = |\psi_t\rangle. \tag{2}$$

The Schrödinger equation for the extended state is then given by

$$\left(i\hbar\frac{\partial}{\partial t} + i\hbar\frac{\partial}{\partial s}\right)|\widetilde{\psi}_{t,s}\rangle = H_t|\widetilde{\psi}_{t,s}\rangle \tag{3}$$

or, equivalently,

$$i\hbar\frac{\partial}{\partial t}|\widetilde{\psi}_{t,s}\rangle = \mathcal{H}_{t,s}|\widetilde{\psi}_{t,s}\rangle \tag{4}$$

with the Floquet-type operator $\mathcal{H}_{t,s} \equiv H_t - i\hbar\frac{\partial}{\partial s}$.

B. Formulation of quasiperiodic quantum dynamics

Now we assume the Hamiltonian to be of quasiperiodic property. In so doing, our formalism deviates from that in Ref. [35]. We first introduce an extended Hamiltonian $\widetilde{H}_{t,s}$ that is dependent on the two time variables. It has a formal periodicity in the second variable s in the sense

$$\widetilde{H}_{t,s+T} = \widetilde{H}_{t,s}, \tag{5}$$

where the fundamental period T is assumed to be a fixed constant.[1] The t-variable dependence of the extended Hamiltonian $\widetilde{H}_{t,s}$ is arbitrary except that it is assumed to have a time scale T_{np} (np stands for nonperiodic) much longer than T ($\frac{T}{T_{np}} \ll 1$) so that the Hamiltonian H_t is quasiperiodic in the sense $H_{t+T} = H_t + O(\frac{T}{T_{np}})$. The physical Hamiltonian is related to $\widetilde{H}_{t,s}$ by

$$H_t = \widetilde{H}_{t,s}|_{s=t}. \tag{6}$$

An example of the Hamiltonian of this property is that of a system under a time-dependent optical field,

$$H_t = H_0 - \boldsymbol{\mu}\cdot\boldsymbol{\varepsilon}E(t)\cos\omega t, \tag{7}$$

where H_0 is the time-independent part, $\boldsymbol{\mu}$ and $\boldsymbol{\varepsilon}$ are the dipole operator and field polarization vector, respectively. The field amplitude $E(t)$ varies slowly with the variable t over multiple optical periods. One can then construct a two-time counterpart of this Hamiltonian as

$$\widetilde{H}_{t,s} = H_0 - \boldsymbol{\mu}\cdot\boldsymbol{\varepsilon}E(t)\cos\omega s, \tag{8}$$

which has formal periodicity in the variable s for a fixed value of t, and is related to the original Hamiltonian by Eq. (6).

Let $\mathcal{R}_t$ collectively represent slowly varying system parameters. It can be readily seen that a two-time extended Hamiltonian of the form $\widetilde{H}_s(\mathcal{R}_t)$, which is periodic in the variable s and dependent on the variable t only through $\mathcal{R}_t$, has the same type of periodicity. The parameters most relevant for the later discussions are the nuclear positions, represented by a collective vector $\mathbf{R} = (\mathbf{R}^1, \mathbf{R}^2, \ldots, \mathbf{R}^N)^T$, with each $\mathbf{R}^I$ being the position of Ith nucleus. The other examples are laser parameters such as the field amplitude and the polarization, which are formally represented as ζ^μ [see Eq. (13)].

In this paper, laser frequency ω is assumed to be a constant, although it can also be among time-dependent parameters as in the case of chirped pulse. Extension of our formalism to such more general cases is discussed in Appendix A.

Substituting the parametrized Hamiltonian $\widetilde{H}_s(\mathcal{R}_t)$ into Eq. (4), the Floquet-type operator becomes $\mathcal{H}_s(\mathcal{R}_t) = \widetilde{H}_s(\mathcal{R}_t) - i\hbar\frac{\partial}{\partial s}$, which is now a true Floquet operator in the sense that it has the exact periodicity in the variable s. It thus follows that the eigenstates of this Floquet operator $\mathcal{H}_s(\mathcal{R}_t)$ are also periodic in the variable s. We define parametrized Floquet states

$$\mathcal{H}_s(\mathcal{R}_t)|\Phi_\alpha(s);\mathcal{R}_t\rangle = \lambda_\alpha(\mathcal{R}_t)|\Phi_\alpha(s);\mathcal{R}_t\rangle, \tag{9}$$

where $\lambda_\alpha(\mathcal{R}_t)$ is the αth Floquet quasienergy. Restricting our attention to the discrete spectrum, we can further impose mutual orthonormality with respect to the inner product $\langle\langle\cdot\rangle\rangle$ defined as

$$\langle\langle u|v\rangle\rangle \equiv \int_0^T \frac{ds}{T}\langle u_s|v_s\rangle, \tag{10}$$

[1] This restriction can be lifted to allow frequency modulations as is shown in Appendix A.

where T is the fundamental period as indicated in Eq. (5).

We now consider an electron-nucleus coupled system. We denote the two-time extension of the total state as $\widetilde{\Psi}_{t,s}$. The corresponding Schrödinger equation, in the nuclear coordinate representation, becomes

$$i\hbar\left(\frac{\partial}{\partial t}+\frac{\partial}{\partial s}\right)\langle\mathbf{R}|\widetilde{\Psi}_{t,s}\rangle=\left[\sum_I\frac{1}{2M_I}\left[\frac{\hbar}{i}\frac{\partial}{\partial\mathbf{R}^I}-\frac{Q_I}{c}\mathbf{A}\right]^2+U_{\rm nuc}(\mathbf{R},t)+\widetilde{H}_s^{\rm ele}(\mathcal{R}_t)\right]\langle\mathbf{R}|\widetilde{\Psi}_{t,s}\rangle, \tag{11}$$

where $\langle\mathbf{R}|$ is the bra vector associated with the position eigenstate of nuclei $|\mathbf{R}\rangle$, M_I and Q_I are the mass and charge of the Ith nucleus, and $U_{\rm nuc}(\mathbf{R},t)$ is the nuclear potential term. $\mathbf{A}$ is the vector potential. Throughout this paper, optical fields are treated within the long-wavelength approximation. $\widetilde{H}_s^{\rm ele}(\mathcal{R}_t)$ is the electronic Hamiltonian including electron-nucleus interactions. We then define the Floquet states $\{|\Phi_\alpha(s);\mathcal{R}_t\rangle\}$ as the eigenstates of the electronic Floquet operator $\mathcal{H}^{\rm ele}\equiv\widetilde{H}^{\rm ele}-i\hbar\frac{\partial}{\partial s}$. The parameter set $\mathcal{R}_t$ in this problem therefore includes nuclear coordinate in addition to laser parameters. The total state $\widetilde{\Psi}_{t,s}$ is then expanded in the form

$$|\widetilde{\Psi}_{t,s}\rangle=\sum_\alpha\int d\mathbf{R}|\mathbf{R}\rangle|\Phi_\alpha(s);\mathcal{R}_t\rangle\chi_\alpha(\mathbf{R},t), \tag{12}$$

where $\chi_\alpha(\mathbf{R},t)$ is the nuclear wave function associated with the electronic state $|\Phi_\alpha(s);\mathcal{R}_t\rangle$. Then the coupled Schrödinger equations for $\chi_\alpha(\mathbf{R},t)$ become

$$i\hbar\dot{\chi}_\alpha(\mathbf{R})=\sum_I\frac{1}{2M_I}\sum_\beta\left(\left[\frac{\hbar}{i}\frac{\partial}{\partial\mathbf{R}^I}-\frac{Q_I}{c}\mathbf{A}-i\hbar\mathbf{X}\right]^2\right)_{\alpha\beta}\chi_\beta+U_{\rm nuc}(\mathbf{R})\chi_\alpha+\lambda_\alpha\chi_\alpha-i\hbar\sum_\mu\dot{\zeta}^\mu\sum_\beta\mathcal{X}_{\alpha\beta}^{(\zeta^\mu)}\chi_\beta, \tag{13}$$

where $\mathbf{X}_{\alpha\beta}^I\equiv\langle\langle\Phi_\alpha|\frac{\partial}{\partial\mathbf{R}_I}|\Phi_\beta\rangle\rangle$ are the nuclear derivative coupling terms, while $\mathcal{X}_{\alpha\beta}^{(\zeta^\mu)}\equiv\langle\langle\Phi_\alpha|\frac{\partial}{\partial\zeta^\mu}|\Phi_\beta\rangle\rangle$ are nonadiabatic coupling terms that are associated with laser parameters ζ^μ.

In this paper, the notion of (non)adiabaticity is meant to be the (non)stationarity of the Floquet states. Under the exact periodicity and in the absence of nuclear derivative couplings, the Floquet theorem ensures the stationarity of Floquet states. Conversely, any deviation from the periodicity can cause transitions among the Floquet states, which are, in our present formalism, uniformly treated as the generalized nonadiabatic transitions [see the first and the last terms in the right-hand side of Eq. (13)].

Equation (13) is basically similar to Eq. (12) in Ref. [34], as it should be. However, the present formalism brings about some key notions and quantities in more definite ways. Some of the examples are the formal periodicity of the Floquet operator $\mathcal{H}_s(\mathcal{R}_t)$ and the formal definition of the inner product, Eq. (10). Both are defined under a fixed value of t, and hence are independent of the t dependence of parameters $\mathcal{R}_t$. This formal independence ensures broader applicability of the present formalism. In fact it is formally applicable even in the cases with poor periodicity, $T/T_{np}\sim 1$.[2] In practice, however, as nonperiodicity T/T_{np} grows, nonadiabatic contributions in Eq. (13) become larger, and hence the advantages of Floquet state expansion diminish. In this regard, the quasiperiodicity in our formalism is not a core assumption but a requirement for an effective use of this method.

In the present formalism, the Floquet-type analysis is applied to the electronic Hamiltonian H^{el}, but not to the total Hamiltonian. As a consequence, the electronic states are expanded in the (parametrized) electronic Floquet basis, which are the eigenstates of the electronic Floquet operator. It thus follows that the eigenvalues are real if possible ionization processes are ignored. If, on the other hand, we used the total Hamiltonian (including the nuclear kinetic part) in constructing the Floquet Hamiltonian, the total state would be expanded in the electron-nucleus coupled Floquet basis. The eigenvalues would be complex-valued reflecting finite dissociation rates. This latter type of treatment has been studied [33,36,37] to reach many important results including lifetime analysis of bond hardening [33], time-independent analysis of photodissociation [36], and discussions on the exceptional points which induce intriguing quantum dynamics [37]. In the present work, however, we take the former approach to take full advantages of the well-established formalism of nonadiabatic dynamics.

C. Physical observables

The two-time extended state $|\widetilde{\psi}_{t,s}\rangle$ bears arbitrariness in the variable s. In the dynamical calculations, an arbitrariness exists in the s dependence of the initial ($t=0$) extended-state vector, $|\widetilde{\Psi}_{t=0,s}\rangle$, which can be set to any function as long as the extended state equals the physical initial state vector $|\Psi_0\rangle$ at $s=0$, that is, $|\widetilde{\Psi}_{t=0,0}\rangle=|\Psi_0\rangle$. For example, two extreme choices are $|\widetilde{\Psi}_{0,s}\rangle=|\Psi_0\rangle\delta(s)$ and $|\widetilde{\Psi}_{0,0}\rangle=|\Psi_0\rangle$ (independent of s).

The s dependence can be fixed for the sake of convenience in actual calculations. This arbitrariness, however, should not affect the final result as far as the "physical observables" are concerned, which are quantities obtained from the physical state vector $|\widetilde{\Psi}_{t,t}\rangle$. It is then clear from the above two extreme choices that the population of an individual Floquet state is not a physical observable and is indeed affected by the choice of the s dependence of an initial state. In order to proceed, we recall that for any Floquet state $|\Phi_\alpha(s)\rangle$ with quasienergy λ_α, scalar multiplication of $e^{-in\omega s}$ yields another Floquet state with a quasienergy $\lambda_\alpha-n\hbar\omega$, which is hereafter referred to as an "$n\omega$ shift" of the original one. We also describe any two Floquet states to be "distinct" if one of them is not an $n\omega$ shift of the other. To obtain physical observables related to the Floquet state population, we consider the following summation over $n\omega$ shifts:

$$\xi_\alpha(\mathbf{R},t)=\sum_n e^{-in\omega t}\chi_{\alpha-n\omega}(\mathbf{R}), \tag{14}$$

[2]This is in contrast to the derivation of Ref. [34], in which smallness of t dependence is explicitly assumed in formulation [see derivation of Eq. (12) of Ref. [34]].

which is the projected amplitude of physical state vector $\langle \mathbf{R}|\widetilde{\Psi}_t(s)\rangle|_{s=t}$ on the Floquet eigenstate at $s=t$; $|\Phi_\alpha(s);\mathcal{R}_t\rangle|_{s=t}$, and is a physical observable. Taking square and neglecting the fast oscillating components (or equivalently, taking an average over one optical cycle), we obtain

$$\rho_{[\alpha]}(\mathbf{R},t) = \sum_n |\chi_{\alpha-n\omega}(\mathbf{R})|^2, \tag{15}$$

where the subscript $[\alpha]$ indicates that the state α and its all $n\omega$ shifts are not mutually distinguished.

D. On the validity of quasiclassical approximation

Having formulated a generalized Floquet Hamiltonian method, we examine the validity of the gradient approximation on quasienergy surface (QES)[3]—an approximation for the nuclear dynamics by classical dynamics of a pointlike particle driven by the minus of the gradient of a single QES.

Using a formal theory of mixed quantum classical representation of nonadiabatic dynamics [38] developed in Ref. [39] (also see Appendix B) [40], the effective force acting on nuclei is given as

$$\mathbf{F}^{\rm eff} \approx \langle \Phi_\alpha(t);\mathcal{R}_t|\left(-\frac{\partial H^{el}}{\partial \mathbf{R}}\right)|\Phi_\alpha(t);\mathcal{R}_t\rangle, \tag{16}$$

provided that the effects of nonadiabatic transitions are negligible. Further assuming that the time scale of nuclear dynamics is large compared to the fundamental period T, we can take the cycle average of Eq. (16) to obtain

$$\mathbf{F}^{\rm eff} \approx \langle\langle \Phi_\alpha(t);\mathcal{R}_t|\left(-\frac{\partial H^{el}}{\partial \mathbf{R}}\right)|\Phi_\alpha(t);\mathcal{R}_t\rangle\rangle = -\frac{\partial \lambda_\alpha(\mathcal{R}_t)}{\partial \mathbf{R}}, \tag{17}$$

which is the gradient of QES.

From this derivation, we obtain three validity conditions for the gradient approximation: (a) smallness of nonadiabaticity (see Appendix B for details), (b) longer time scale of nuclear dynamics, and (c) absence of purely quantum-mechanical effects, such as tunneling, the last one being the assumption in the discussions in Ref. [39].

Conversely, the gradient approximation breaks down around avoided crossings on QESs, where strength of the nonadiabatic coupling becomes large compared to the difference of adjacent quasienergies. Avoided crossings of QESs in the weak-field limit typically occur around resonant points, where the energy difference of two dipole-coupled adiabatic states is equal to $n\hbar\omega$ with n being an integer (referred to as $n\omega$ resonances). Resonant points, along with intrinsic avoided crossings on the original field-free PESs, are to be treated with special care in the following analysis.

[3]In this paper, in order to emphasize the term Floquet quasienergy, we use the term QES, whereas the term "field-induced PES" seems to be more common in the literature.

III. APPLICATIONS TO THE FIELD-INDUCED BOND DEFORMATION OF H_2^+ AND D_2^+

To verify the theory presented above, we have implemented Eq. (13) in a computational scheme to actually obtain the extended wave function $\widetilde{\Psi}_{t,s}$. We first examine the method with the field-induced dynamics of H_2^+ and D_2^+, in which no nuclear derivative coupling is involved, and then in the next section we present a unified treatment of field-induced nonadiabatic dynamics and the intrinsic one due to the nuclear kinetic couplings in the LiF molecule. Most of the technical details described in this section, except for the potential functions and coupling elements, are also applied to the study of LiF in the next section.

A. Systems and computational methods

The field-induced dynamics of H_2^+ and D_2^+ has been intensively studied in the literature and hence the properties are well known to serve as reference data. For the simplest assessment of the method, we use the two-state model proposed in Ref. [41]. The two-state models are known to sufficiently reproduce the essential effects in the field-induced bond dynamics: bond softening and bond hardening. We can therefore check if these two fundamental effects are correctly treated in the present method. The R-dependent electronic states are denoted as $|j;R\rangle$, with either $j=g$ or $j=u$ corresponding to the gerade and ungerade states, respectively. The molecular orientation is fixed so as the molecular axis is parallel to the polarization vector of the applied laser in, say, the x axis, and we concentrate only on the one-dimensional vibrational motion. The Schrödinger equation is

$$i\hbar\frac{\partial}{\partial t}\Psi_\alpha(R) = \sum_\beta\left[-\frac{\hbar^2}{2M}\frac{\partial^2}{\partial R^2}\delta_{\alpha\beta} + H^{\rm ele}_{\alpha\beta}(R,t)\right]\Psi_\beta(R), \tag{18}$$

where M is the reduced mass of the nuclear relative motion and $H^{\rm ele}$ is the electronic Hamiltonian given as

$$H^{\rm ele}(R,t) = \begin{pmatrix} U_g(R) & -\mu(R)E(t)\cos(\omega t) \\ -\mu(R)E(t)\cos(\omega t) & U_u(R)\end{pmatrix} \tag{19}$$

with $E(t)\cos(\omega t)$ being the electric field, and $\mu(R)$ is the dipole matrix element between the g and u state. Here the electric-field amplitude $E(t)$ is chosen to be of a single Gaussian form with the full width half maximum (FWHM) being 150 fs; $E(t)=E_0\exp[-(\frac{t-t_c}{t_w})^2]$ with $t_c=162.15$ fs and $t_w=90.08$ fs. The effective potential and the dipole matrix element are, following Ref. [41], given as

$$U_g(R) = K\{\exp[-2D(R-R_0)] - 2\exp[-D(R-R_0)]\}, \tag{20}$$

$$U_u(R) = K\{\exp[-2D(R-R_0)] - 2a\exp[-D(R-R_0)]\}, \tag{21}$$

$$\mu(R) = \mu_0 + \frac{\mu_0'}{Dy}\{1-\exp[-Dy(R-R_0)]\}. \tag{22}$$

Here the parameters are set, following Ref. [41], as $D = 0.72$, $K = 0.10262$, $R_0 = 2.0$, $\mu_0 = 1.07$, $\mu_0' = 0.396$, $y = -0.055$, and $a = -1.11$, respectively. We use the atomic units throughout, except for time.

The Schrödinger equation (18) was numerically solved using a standard grid-based split operator method [42]. Each $\chi_\alpha(\mathbf{R})$ in Eq. (13) is represented on a spatial grid. Although this implementation scarifies applicability to larger systems, we can expect the most accurate results that are directly comparable to those obtained by full quantum calculations. Here the one-dimensional space is limited to the range $[0, R_{\max}]$ and divided into N_S equal-spaced lattice, whose lattice points are given as $R_k = k\frac{R_{\max}}{N_S}$, $k = 0, \ldots, N_S - 1$. The actual parameters used are $N_S = 4096$ and $R_{\max} = 20$. The results were confirmed to be qualitatively independent of the system size by comparison with those of a smaller size simulation $N_S = 2048$ and $R_{\max} = 16$. An imaginary potential term V_I is applied near the boundary in order to eliminate unphysical reflections by absorption:

$$V_I = \begin{cases} -iB_0\left(\frac{R-R_b}{R_w}\right)^2 & R_a \leqslant R \leqslant R_b, \\ 0 & \text{otherwise}, \end{cases} \tag{23}$$

where we chose $B_0 = 2.4K$ [this K is the parameter introduced in Eq. (20)], $R_w = 3.6$, $R_a = 14.0$, and $R_b = 18.0$.

The extended state $|\widetilde{\Psi}_{t,s}\rangle$ is propagated using the Trotter formula [see Eq. (24) below]. We use the Fourier series expansion to represent the s dependence of the extended state as $|\widetilde{\Psi}_{t,s}\rangle = \sum_n e^{-in\omega s}|\widetilde{\Psi}_t^F[n]\rangle$, where $|\widetilde{\Psi}_t^F[n]\rangle$ represents the nth Fourier component of the extended state vector, and n runs from $-N_w$ to N_w with a fixed large number N_w for the cutoff (actually set to 50). The Fourier series is then represented in the column vector as $|\widetilde{\Psi}_t^F\rangle = (|\widetilde{\Psi}_t^F[-N_w]\rangle, |\widetilde{\Psi}_t^F[-N_w+1]\rangle, \ldots, |\widetilde{\Psi}_t^F[N_w]\rangle)^{\mathrm{T}}$, where the superscript T indicates the vector transposition. We then have

$$\left|\widetilde{\Psi}_t^F\right\rangle = \prod_{j=0}^{P-1}\{e^{-(i/\hbar)(\epsilon/2)\mathbf{T}^{\mathrm{nuc}}} e^{-(i/\hbar)\epsilon\mathbf{H}^{\mathrm{eff}}(t_j)} e^{-(i/\hbar)(\epsilon/2)\mathbf{T}^{\mathrm{nuc}}}\}\left|\widetilde{\Psi}_0^F\right\rangle, \tag{24}$$

where P is the number of the time steps in the Trotter decomposition, $\epsilon \equiv \frac{t}{P}$ is the infinitesimal time step, $t_j \equiv j\epsilon$ is the jth time point, $\mathbf{T}^{\mathrm{nuc}}$ and $\mathbf{H}^{\mathrm{eff}}(t_j)$ are the Fourier series representation of the nuclear kinetic term T^{nuc} and the effective electronic Hamiltonian $H^{\mathrm{eff}} \equiv \mathcal{H}^{\mathrm{ele}} + \mathbf{V}_I$ in a matrix form, respectively. In the actual computation, the nuclear kinetic term was calculated using the fast Fourier transformation (FFT) technique [42]. The electronic state was expanded with the Fourier-transformed diabatic basis; $e^{-in\omega s}|j;\mathbf{R}\rangle$. The total state in this representation has the form $|\widetilde{\Psi}\rangle = \sum_j \sum_k \sum_{n=-N_w}^{N_w} e^{-in\omega s}|\mathbf{R}_k\rangle|j;\mathbf{R}_k\rangle\chi_{j,k}[n]$, where $\chi_{j,k}[n]$ is the nth Fourier series component of the discretized nuclear wave function $\chi_{j,k} \equiv \chi_j(R_k)$.

The initial conditions of the present dynamical simulation are chosen such that the electronic state is in the ground (gerade) state and the nuclear state is at one of the vibrational eigenstates (quantum number v) of the gerade electronic state. The corresponding extended-state vector at $t = 0$ is then fixed as $\chi_{j,k}[n] = \delta_{j,g}\delta_{n,0}\phi_v(R_k)$, with the vth vibrational eigenstate wave function $\phi_v(R)$. As stated above, the initial choice of the extended state at $t = 0$ has arbitrariness with respect to the dependence on the variable s. The choice here corresponds to $|\widetilde{\Psi}_{t=0,s}\rangle = |\Psi_0\rangle$ (independent of s) and is found to be favorable for the present numerical implementation, since by this choice (together with the only weakly nonperiodic nature of the problem) only a small number of states in n is populated during the whole simulation. The simulation starts at $t = 0$ fs and end at $t \gtrapprox 400$ fs. The duration of simulation time is taken long enough. (We recall that the pulse is Gaussian of FWHM = 150 fs centered at $t_c = 162.15$ fs.)

The Floquet state population at an arbitrary time point is obtained by projecting the extended state vector on the Floquet eigenstate vector, which is obtained by diagonalization of the Floquet operator $\mathcal{H}^{\mathrm{ele}}$. Formally, the physically meaningful quantity should be given as in Eq. (14). However, within the parameters chosen in this study the Floquet states of the higher order are scarcely populated. Therefore the summation in Eq. (14) was replaced with a single term.

B. Dissociation probability and underlying wave-packet dynamics

We first show the calculated dissociation probability in Fig. 1. The results for H_2^+ are in good agreement with Fig. 18 of Ref. [43], in which no further analysis has been reported. As we notice in Fig. 1, the dissociation probability versus the field

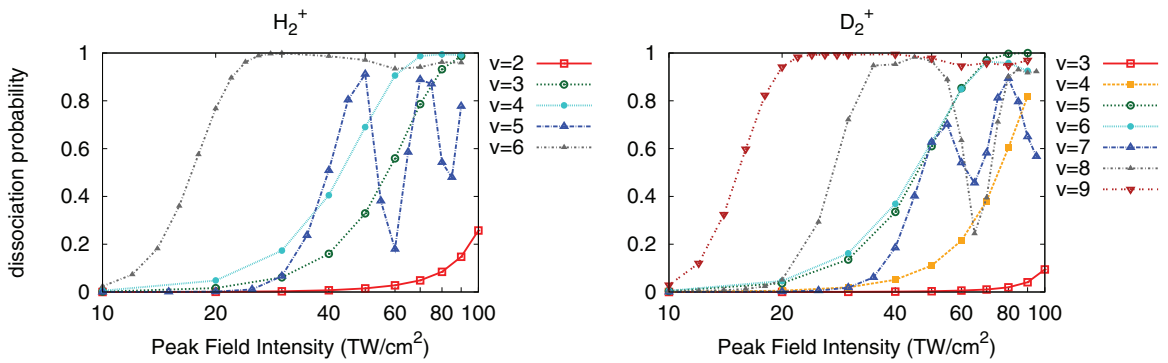

FIG. 1. (Color) The dissociation probability calculated from the total population lost from the simulation space $0 \leqslant R \leqslant R_{\max}$ during the laser radiation. Left and right panels show the results for H_2^+ and D_2^+, respectively. Each line shows the result obtained from the initial vibration state indicated on the right of each panel. The horizontal axis is plotted in log scale.

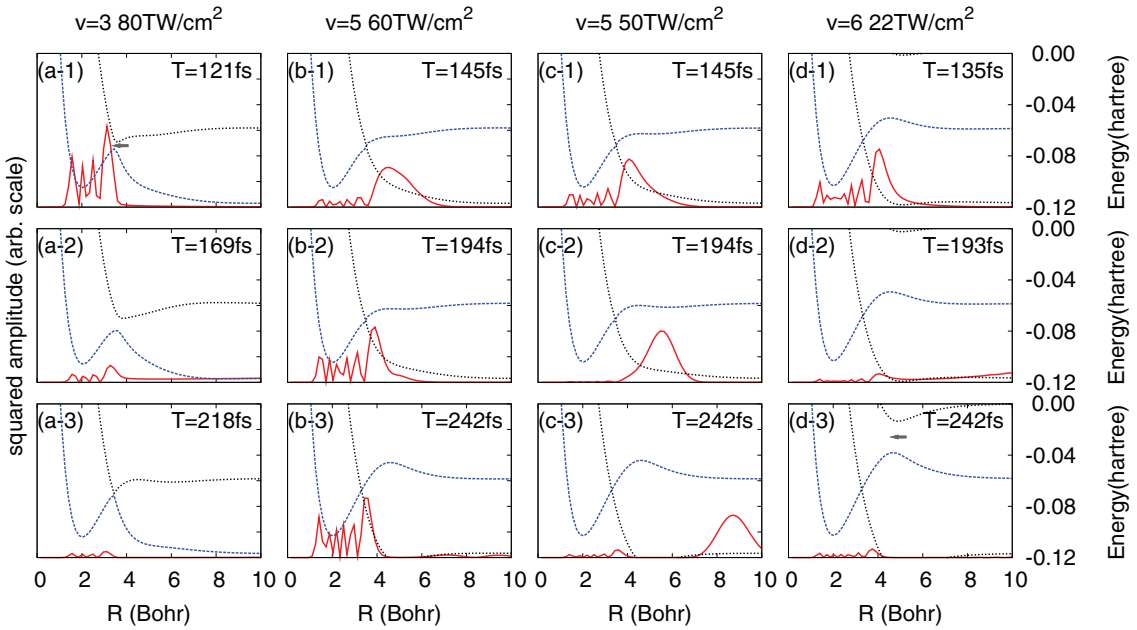

FIG. 2. (Color online) Snapshots of the squared wave-packet amplitude and Floquet quasienergy surface. Each panel shows the snapshot at the time point which is indicated at the right top. For each panel, the red solid line represent the squared amplitude of the dominant Floquet state, and the blue dashed curve represents the corresponding quasienergy surface. Another closely related QES is also plotted with black dotted line for reference. Three panels in each vertical row show snapshots of the dynamics starting from the initial vibrational state and the peak field intensity indicated at the top. We also plotted approximate position of resonant points by gray arrow. The arrow in panel (a-1) shows the 3ω resonance point while that in panel (d-3) shows 1ω resonance point.

intensity are classified into three overall patterns. Pattern 1: Near-zero probability at low field followed by rapid monotonic increase at higher intensity: $v = 2,3,4$ in H_2^+ and $v = 3,4,5,6$ in D_2^+. Pattern 2: Nonmonotonic oscillatory behavior; $v = 5$ in H_2^+ and $v = 7,8$ in D_2^+. Pattern 3: Similar to pattern 1, but the increase occurs at much lower field; $v = 6$ in H_2^+ and $v = 9$ in D_2^+.

In order to analyze the dynamics behind each pattern, we show in Fig. 2 selected snapshots of wave packets represented by the squared amplitude of the dominant Floquet state. The time-dependent behavior of the related QESs are also superimposed in the figure. One can observe that the wave-packet motion is in accordance with the QES gradient, thereby qualitatively verifying the quasiclassical interpretation. Throughout the present simulation, the population of the $n\omega$ shifts of the dominant Floquet state was negligibly small in the entire parameter range. The population of the second-dominant Floquet state, which is distinct from the dominant one, is also negligible in the parameter region in Fig. 2. The second-dominant state population, however, may grow to a finite value in other parameter regions (not plotted) especially around the resonant points. Discussions below are about the mechanisms of the above phenomena, which are based on the dominant state behavior only, nonetheless characterizing the overall behavior.

1. *Pattern 1: Bond softening*

The snapshots of the dynamics of initial state $v = 3$ and the peak field intensity $I = 80$ TW/cm^2 are shown in the three panels, (a-1)–(a-3) in Fig. 2, where one can see that the wave packet moves out through deformed QES after the opening of the gap at the 3ω resonant point, which is a typical behavior in bond softening [43]. Dynamics in other parameters categorized in this pattern also shows a similar behavior at intensities higher than an onset intensity, where a sharp increase of dissociation probability (see Fig. 1) occurs. We thus identify the present pattern as bond softening.

2. *Pattern 2: Bond hardening and inverse bond hardening*

The snapshots of the wave-packet dynamics of $v = 5$ at the peak field intensity $I = 60$ TW/cm^2, which is at the bottom of the dissociation probability oscillation (see Fig. 1), are shown in panels (b-1)–(b-3) of Fig. 2. One can see that the increase of the QES local maximum near the 1ω resonant point prevents the wave packet from dissociation, which is a typical behavior in bond hardening [29,33,43,44].

We also show, in panels (c-1)–(c-3) in Fig. 2, the snapshots of the dynamics of $v = 5$ with the peak field intensity $I = 50$ TW/cm^2, which is at the peak of the dissociation probability oscillation. Here the development of a local maximum in QES near the 1ω resonant point seems to push out a portion of the wave packet. Hence the underlying mechanism is the same as the normal bond hardening seen in the dynamics at the peak field intensity $I = 60$ TW/cm^2, although the outcome is opposite. We thus term it "inverse bond hardening."

3. *Pattern 3: Bond softening (at 1ω resonant point)*

The snapshots of the dynamics of $v = 6$ at the peak field intensity $I = 22$ TW/cm^2 are shown in panels (d-1)–(d-3) in Fig. 2. Here we can see the wave packet move out through the gap formed by the 1ω resonance. The onset occurs at much lower intensity due to the stronger dipole coupling

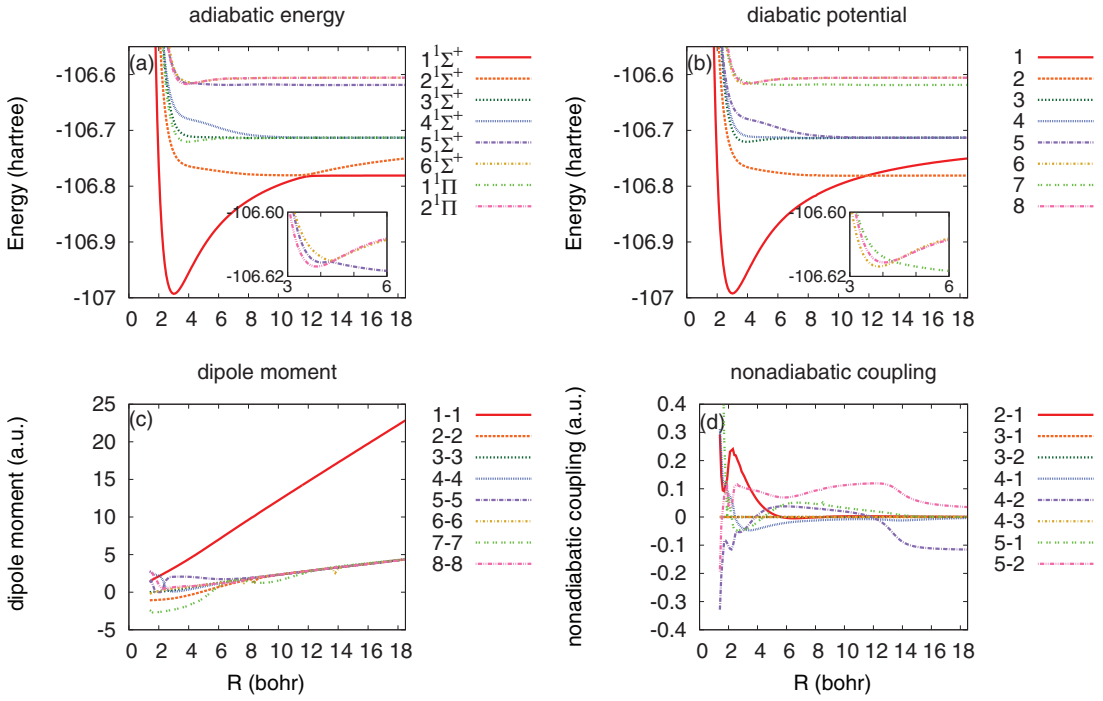

FIG. 3. (Color) The adiabatic PESs (a) and the relevant elements (b)–(d) of matrices obtained by *ab initio* calculations. Matrices in (b)–(d) are in the approximate diabatic representation as described in the text. (a) Adiabatic energies of the lowest eight adiabatic states. (b) Diagonal elements of the Hamiltonian matrix. (c) Diagonal elements of the electric dipole matrix. (d) Off-diagonal elements of the nuclear nonadiabatic coupling matrix. The adiabatic states are labeled as $1^1\Sigma^+$ to $6^1\Sigma^+$, $1^1\Pi$, $2^1\Pi$, where numbers are given in an increasing order in the adiabatic energies.

at the 1ω resonant point than that at the 3ω resonant point. Nevertheless, the essential mechanism is bond softening, the same as pattern 1.

To summarize this section, we have thus verified the present formalism by successfully reproducing the dissociation probabilities of H_2^+ reported in Ref. [43], including the oscillatory feature. We also show that an interplay of bond softening and bond hardening can be clearly seen in the snapshots of time-dependent QESs and wave-packet dynamics on them, which is clearly understood in terms of quasiclassical approximation. In fact our simulation serves as a direct real-time demonstration of possibly competing bond-softening and bond-hardening mechanisms, and moreover, has suggested a possible phenomenon, the inverse bond-hardening.[4] The additional calculations for D_2^+ dissociation have been found to be consistent with these interpretations.[5]

IV. APPLICATION TO THE CURVE-CROSSING DISSOCIATION DYNAMICS OF LiF

We next proceed to a system in which the intrinsic nuclear derivative couplings directly affect the dissociation process in laser fields. We take LiF as a case study having an avoided crossing of ionic and covalent PESs [see Fig. 3(a)]. In the presence of strong laser field, these ionic and covalent PESs are expected to be largely deformed, since these two and other possible excited states are dipole coupled. Thus a qualitative description of the field-induced dissociation dynamics should require full consideration of nuclear kinematic effects as well as dynamical deformation of QESs.

A. Systems and computational details

Theoretical studies on LiF in recent years include static *ab initio* calculation of PESs [45,46], and calculations of field-induced dynamics [47,48]. To the best of our knowledge, no experimental study on its field-induced dynamics has ever been reported, but it still serves as a prototype for studying an interplay of field-induced and intrinsic nonadiabatic transitions.

The full quantum-mechanical calculations in Ref. [47] suggests onset of dissociation under strong infrared ($\lambda = 9.4\ \mu$m) laser field of order 10^0–10^1 TW/cm^2. Mixed quantum classical calculations in Ref. [48], on the other hand, show dissociation under higher field intensities around 10^2–10^3 TW/cm^2 although the laser wavelengths are different from Ref. [47]. Here we consider the laser field of wavelength $\lambda = 227$ nm.

1. *Ab initio calculation of electronic matrix elements*

We first calculate PESs and relevant matrix elements of LiF by *ab initio* calculations. We use the program package GAMESS

[4]Further discussions on physical conditions are necessary for inverse bond hardening, bond softening, and bond hardening to be observed experimentally.

[5]In fact the spatial distribution of the initial wave function with respect to the position of the QES resonant points is found to have similarity among each pattern. The fact may explain the origin of each pattern, but will be discussed elsewhere.

[49] to perform configuration interaction calculations limited to single and double excitation (CISD) using the graphical unitary group approach (GUGA) [50] and obtain PESs as well as the relevant matrix elements including electronic dipole and derivative couplings [51]. Our chosen basis set is Dunning's second-order augmented correlation-consistent basis set (aug-cc-pCVDZ) [52], which generates a total of 48 atomic orbitals. In the CISD calculations, 2 core-like and 27 higher-lying orbitals out of 48 molecular orbitals are frozen. The number of symmetry-adapted configuration state functions (CSFs) was 870.

The adiabatic PESs are shown in Fig. 3. Although the calculation level is rather lower than the previous works on the same molecule [46], it is however sufficient to qualitatively reproduce the features obtained from more accurate calculations [46]. The position of the avoided crossing of the lowest two PESs is obtained at around internuclear distance $R_c = 11.85$. (Reference [46] reports $12 \leqslant R_c \leqslant 13$ with larger size calculations.) Since the value of R_c is sensitive to the level and size of calculations, the present R_c seems to be within a tolerable range. The necessary matrix elements in the adiabatic representation are first calculated using the $N_{\rm tot} = 870$ CSFs as described above. Dimension of the basis set is then reduced by restricting to the lowest $N_b = 8$ adiabatic states.

The obtained $N_b \times N_b$ matrices are further transformed to an approximately diabatic basis to avoid the direct use of the derivative couplings. Here an approximate diabatization is applied to the lowest two adiabatic states, whereas the rest $N_b - 2$ basis states are kept as adiabatic states. We diagonalize the lowest 2×2 block of the dipole matrix to obtain new states with either "ionic" or "covalent" character. Thus the nonadiabatic coupling between these states has been significantly reduced around the avoided crossing, although being finite. The residual derivative couplings are evaluated as is separately described in Appendix C.

The relevant elements of thus obtained matrices are shown in Fig. 3. All the matrices are calculated at 171 grid points with the internuclear distance $R^{(p)} = 1.4 + 0.1p$ ($p = 0,1,2,\ldots,170$).

2. *Quantum wave-packet calculations*

Here again we assume one-dimensional nuclear motion along the molecular axis, which is fixed parallel to the field polarization. The quantum wave-packet calculations are then performed using Eq. (24) in a similar manner as was described in the preceding section but with several modifications. The nuclear degrees of freedom is represented by internuclear distance R, whose corresponding reduced mass is $M_{\rm eff} = \frac{M_{Li}M_F}{M_{Li}+M_F}$ and the effective charge $Q_{\rm eff} = \frac{M_F Q_{Li} - M_{Li} Q_F}{M_{Li}+M_F}$, which are, in the atomic unit, 9265.97 and $-0.591\,950$, respectively.

The grid points are chosen as $R = R_{\rm min} + k\frac{R_{\rm max}-R_{\rm min}}{N_S}$ with $k = 0,1,\ldots,N_S - 1$, $R_{\rm min} = 1.4$, and $R_{\rm max} = 18.312$. The number of grid points N_S is set to 2048. An imaginary potential term of the form Eq. (23) is applied with modified parameters: $B_0 = 0.5084$, $R_a = 16.312$, $R_b = 18.312$, and $R_w = 2.0$. Matrices at each grid point R_k are obtained by a linear interpolation technique using the nearest two data points ($R^{(p)}$ and $R^{(p+1)}$ which satisfies $R^{(p)} \leqslant R_k < R^{(p+1)}$). The cutoff of the Fourier series N_w is set to 30, which is confirmed to be sufficiently large by comparing the results with those of $N_w = 45$.

Due to the existence of finite diagonal components in the dipole matrix, better convergence is expected by using the velocity gauge rather than the length gauge. We calculate the electronic dipole velocity momenta in the adiabatic representation using the formula $\frac{q_e}{m_e}(\mathbf{p})_{\alpha\beta} = \frac{i}{\hbar}(\mathcal{E}_\alpha - \mathcal{E}_\beta)(\boldsymbol{\mu})_{\alpha\beta}$, where m_e and q_e are the electronic mass and charge, respectively, $\mathbf{p}$ and $\boldsymbol{\mu}$ are the electronic momentum and the dipole matrices, and $\mathcal{E}_\alpha$ is the αth adiabatic energy, respectively. We also redefine the field in terms of the vector potential as $A(t)\cos(\omega t)$ with a Gaussian pulse envelope $A(t) = A_{\rm max}\exp[-(\frac{t-t_c}{t_w})^2]$. In this paper, the pulse width is set to 300 fs (FWHM) and t_c and t_w are chosen to be 324.3 and 180.2 fs, respectively. The width is set longer than that used in H_2^+/D_2^+ to take account of the heavier reduced nuclear mass.

To prepare the initial vibrational states, we fit the first diagonal element of the Hamiltonian matrix (this is almost equal to the ground adiabatic surface in the range of R in which the vibrational states of our interest lie) to a Morse potential and derived the vibrational eigenstates.

B. Laser-induced dynamics of LiF

The graph of the dissociation probability against the laser intensity under a pulse of FWHM 300 fs is depicted in Fig. 4. It shows a globally monotonic increase of the dissociation probability with pulse peak intensity, but with a slight oscillatory behavior, which implies the existence of a trapping mechanism. However, this effect is less clear than in the case of H_2^+ and D_2^+.

A typical dissociation process is seen in Fig. 5, which shows the behavior of the Floquet populations and corresponding QESs obtained in the simulation under a laser pulse of width 300 fs (FWHM) and the peak intensity $I = 126.36$ TW/cm^2 ($A_{\rm max}/c = 0.30$). Here again the population of the higher-order Floquet states are small, and therefore we can use the single Floquet state populations to represent the actual dynamics. Note the difference of the topology of QESs between the two panels: the three QESs in panel (a), plotted with orange solid, purple dotted and light green dashed lines correspond to those in panel (b), plotted with red solid, blue

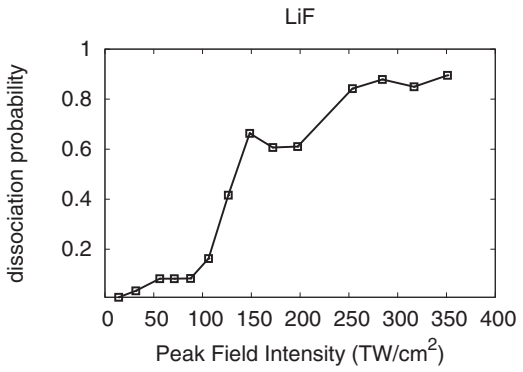

FIG. 4. Dissociation probability calculated from the total population lost from the simulation space $R_{\rm min} \leqslant R \leqslant R_{\rm max}$ during the simulation time. Pulse FWHM was set 300 fs and the initial vibration state was set to $v = 3$.

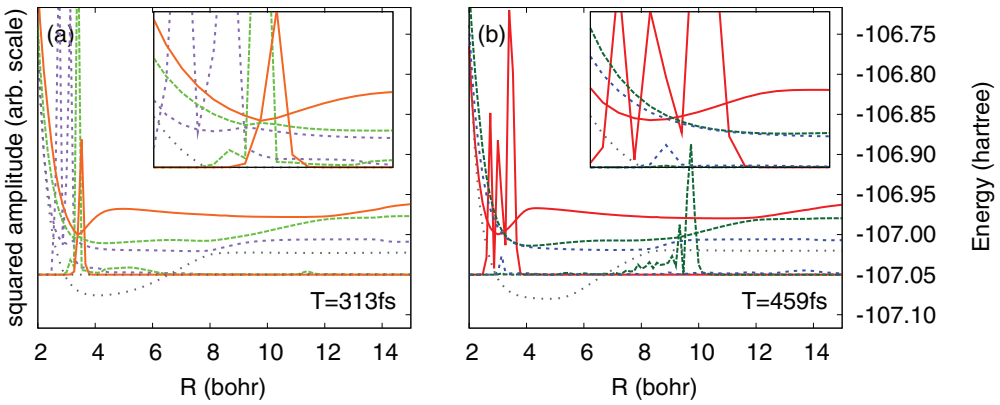

FIG. 5. (Color) The squared Floquet state amplitudes and QESs in the dissociation dynamics of LiF under a laser pulse of width 300 fs (FWHM) and the peak intensity $I = 126.36$ TW/cm^2 ($A_{\max}/c = 0.30$). Each panel shows the snapshot at the time indicated on the panel: (a) $t = 313$ fs and (b) $t = 459$ fs from the pulse onset. The scale for the QES plot is indicated on the right of each panel, while that for the amplitude plot is arbitrary. Each Floquet state population and the corresponding QES is plotted with the same color and the same line style. $1'$: orange solid; $2'$: light green dashed; $3'$: purple dotted lines in panel (a) are related to 1, red-solid (S1); 2, dark green dashed (S2); and 3, blue dotted (S3) lines in panel (b) (see also text). The gray thin dotted curve in each panel, which shows the QES of the fourth dominant Floquet state (S4), is plotted to help understanding although the corresponding state population is almost negligible.

dotted, and dark green dashed lines. The correspondence is one-to-one in the asymptotic region (typically $R \gtrsim 8$), although it is not in the region with small R. For the sake of convenience of later discussion, we label each Floquet state accordingly; those plotted with (1) red solid, (2) dark green dashed, and (3) blue dotted lines will be referred to as the Floquet state S1, S2, and S3, respectively. The wave packet begins to flow out of the initial bound potential ($R \lesssim 4$) around the time when the laser pulse intensity reaches the peak. An example is seen in Fig. 5(a), in which the field is strong enough to induce significant deformation of QES at even around the equilibrium bond length ($R \approx 3.0$). In panel (a) three QESs avoid-cross around $R \approx 3$ and part of the initially bound vibration state population goes out along the QES plotted by the light green dashed line (see also the inset for details). The dynamics in this region is therefore similar to that in the bond-softening pattern of H_2^+/D_2^+.

In contrast to H_2^+/D_2^+, the outgoing wave packet in this system further undergoes trapping at a "later stage," or at a larger value of R. As is shown in Fig. 5(b), the outgoing wave packet is trapped by the upward slope of the corresponding QES around $8 \lesssim R \lesssim 12$, which essentially comes from the character of the ionic PES. Some proportion on it, on the other hand, undergoes nonadiabatic transition through the avoided crossing at $R \approx 9$ to another Floquet state (a blue dotted curve) of the covalent type and leading to dissociation. We note however that in this simulation, this later-stage trapping at the intermediate region $8 \lesssim R \lesssim 12$ is led to dissociation as the field diminishes.

To facilitate understanding of the above dynamics, we correlate the field induced QESs in Fig. 5 to those in the zero-field limit (ZF QESs), which are field-free PESs and their $n\omega$ shifts [see Fig. 3(a)]. Such an approximate assignment would allow an intuitive characterization of the finite field QESs. Figure 6 presents the QESs of Fig. 5(b) and related ZF QESs. We first study the global features: the upward slope of the QES seen in the region $8 \lesssim R \lesssim 12$ reflects $-\omega$-shifted $1^1\Sigma^+$, whereas the blue dotted QES, which asymptotes to -2ω-shifted $6^1\Sigma^+$, leads to dissociation. We can also see that the QES forming the initial bound state ($1^1\Sigma^+$ or its finite-field correspondence) and those leading to dissociation (-2ω shifted $5^1\Sigma^+$, $6^1\Sigma^+$, or their finite-field correspondence) are indirectly coupled with -2ω shifts. This type of coupling would be zero in the two-state model of H_2^+/D_2^+, but is finite here due to the existence of more than two dipole-coupled states.

We finally survey the role of the nuclear derivative couplings. Since we adopt a diabatic representation for the relevant states that are involved in the avoided crossing under study (see Sec. IV A1), the effects from the nuclear kinematic coupling is generally expected to be small. Nonetheless, our computations taking full account of all the nonadiabatic interactions show definite effects in dynamics as follows: It is expected that the "later stage trapping" observed above should be affected by the kinematically induced nonadiabatic transitions at around the avoided crossing of QESs. In order to confirm this, we perform additional calculations in which the

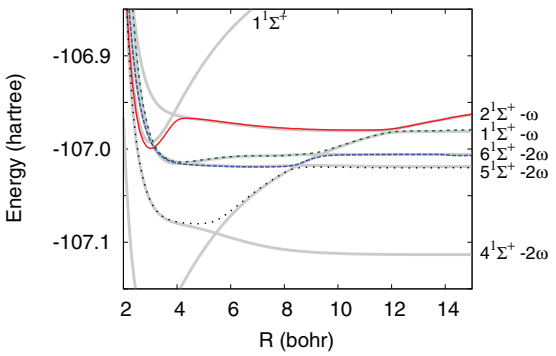

FIG. 6. (Color) The same QESs as Fig. 5(b), with the zero-field limit QESs (ZF QESs) being added in gray lines (refer to Fig. 3). The characters of ZF QESs are indicated in right hand side of the figure. The red solid, blue dotted, and dark green dashed lines, on the other hand, show QESs identical to Fig. 5(b).

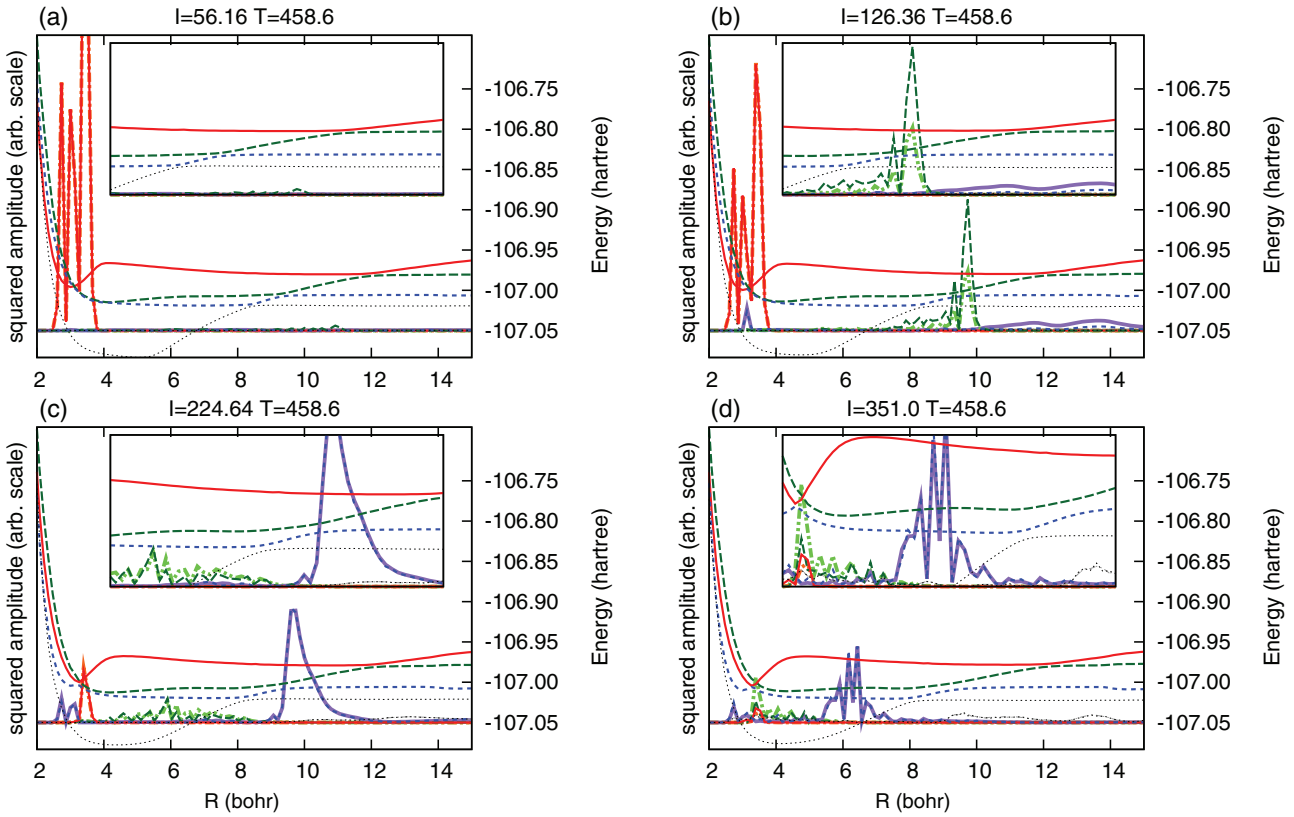

FIG. 7. (Color) Comparison of the squared wave-packet amplitudes between the results obtained by the two calculation schemes (see text). In each calculation, the laser pulse FWHM is fixed at 300 fs and the peak intensity is set (a) $I = 56.16$ TW/cm^2 ($A_{\max}/c = 0.20$), (b) $I = 126.36$ TW/cm^2 ($A_{\max}/c = 0.30$), (c) $I = 224.64$ TW/cm^2 ($A_{\max}/c = 0.40$), and (d) $I = 351.0$ TW/cm^2 ($A_{\max}/c = 0.50$), respectively. The snapshot at fixed time $T = 459$ fs from the pulse onset is taken for comparison. The external conditions for the panel (b) is hence identical to that of Fig. 5(b). The Floquet state populations and their corresponding QESs obtained by the N-scheme calculations are plotted with the same line styles as Fig. 5(b). S1: red full; S2: green dashed; S3: blue dotted; and S4: black thin dotted, respectively, whereas the Floquet state populations in the Z scheme are plotted with S1′: orange dash-dotted; S2′: light-green dash-dot-dotted; S3′: purple dash-dot-dot-dotted; and S4′: gray thin dotted lines, respectively.

nuclear derivative coupling terms [in Eq. (13)] are intentionally ignored (zero nuclear derivative coupling limit denoted as Z scheme). The resultant nuclear wave-packet behavior is shown in Fig. 7, contrasted to that of the full standard calculations of nuclear derivative couplings (N scheme). Figure 7 shows the snapshots of the squared amplitudes and QESs of the relevant Floquet states at each parameter shown in the figure. In particular, panel (b) shows the results obtained at the same parameters as those in Fig. 5(b). The results of the N-scheme calculation is plotted in the same manner as that of Fig. 5(b), whereas the results of Z-scheme calculations are added using orange dash-dotted, light green dot-dot-dashed, and purple dot-dot-dot-dashed lines for the Floquet state S1, S2, and S3, respectively. We first see Fig. 7(b) where the differences of the two schemes are most pronounced. It shows a larger population of state S2 around $R \approx 10$ in the N-scheme result whereas a larger population has leaked off to dissociate through state S3 in the Z-scheme result (compare the purple dot-dot-dot-dashed lines against the blue-dotted ones), indicating enhanced trapping due to the derivative coupling term. The result does not match the naive perturbative expectation; if one assumes the nonadiabatic term as a small perturbation term added on the local Floquet Hamiltonian, any addition of "small" off-diagonal terms would induce transitions among the Floquet states. Such a simple guess, however, does not apply here because the nonadiabatic term is not necessarily a small perturbation at the avoided crossing of Floquet states.

We further compare the result with those obtained in different values of laser parameters. In the weakest peak field amplitude, $I = 56.16$ ($A_{\max}/c = 0.2$), the effect of derivative coupling is negligible because the population passes through the avoided crossings is small. In stronger peak field amplitudes, $I = 224.64$ ($A_{\max}/c = 0.4$) and $I = 351.0$ ($A_{\max}/c = 0.5$), the differences are small. The differences appear to decrease with the peak intensity. This is partly accounted for as the suppression of nonadiabatic transitions by a larger gap among Floquet states.

In principle, the effect of nonadiabatic terms should be small when the (temporal) laser intensity is large and gaps among the Floquet states are large, but it may become relevant otherwise. It is also affected by the "velocity" of the wave packet in the form $i\hbar\mathbf{v}\cdot\mathbf{X}$, where $\mathbf{v}$ is the wave-packet velocity (a more precise description will be given in Appendix D). In dynamics under a pulsed laser field, one can then expect a non-negligible effect if an accelerated wave packet passes

through the avoided crossing on the falling edge of the pulse. The reality is, however, that much is dependent on the details of dynamics.

We must also note that the effects are transient and the total dissociation probability (evaluated at large t from the onset, where laser pulse diminishes) is almost identical between the two schemes. However, the result may differ if there are multiple dissociation channels and one distinguishes between them [1].

We have thus applied our generalized Floquet method on the field-induced dissociation of ionic bound LiF using *ab initio* PESs and matrix elements, and observed that, even in the presence of nuclear derivative couplings, wave-packet dynamics can be qualitatively understood in terms of quasiclassical dynamics on QESs. We have also explicitly shown nontrivial effects of kinematically induced transitions on the wave-packet amplitudes.

V. SUMMARY AND DISCUSSION

We have formulated a generalized Floquet Hamiltonian method that is applicable to dynamics including nonperiodicity arising from time dependence of laser parameters and/or the nuclear kinematic effects. Use of the two-time formalism led to a clear method that is formally independent on the details of the time-dependent parameters. In this method, effects from these two types of nonperiodicity are treated in a unified manner under the notion of generalized nonadiabatic transitions. This unified treatment naturally allows for quasiclassical analysis in the (field-free) nonadiabatic dynamics with use of the gradients of QESs, to which we have given analytic and numerical verification. A numerical implementation of this method has been applied first to the field-induced dynamics of $H_2{}^+/D_2{}^+$ within the two-state model with no derivative coupling. The dissociation probabilities obtained for them have been in good agreement with previously reported results. Analysis of time-dependent QESs and wave-packet dynamics has exposed some more details about the bond softening, bond hardening, and inverse bond hardening. In the second application to the curve-crossing dynamics of LiF, we have performed calculations of the generalized Floquet-based method in the level of *ab initio* electronic states, including the nuclear derivative coupling elements among them. In fact we have shown a nontrivial effect of the intrinsic (kinematic) nonadiabatic interaction in the system of field-induced nonadiabatic dynamics. The present method, giving a simple and clear view of field-induced and intrinsic nonadiabatic transitions, will contribute to the study of laser control of chemical reactions and therefore deserves further study.

ACKNOWLEDGMENTS

This work has been supported by a Grant-in-Aid for Scientific Research from Japan Society for the Promotion of Science (Grant No. 23245002 and in part Grant No. 23 · 9633). One of the authors (K.H.) was supported by a Grant-in-Aid for JSPS Fellows (DC1).

APPENDIX A: EXTENSION TO TIME-DEPENDENT FREQUENCY

In the (generalized) Floquet formalism, the time-dependent variation of the optical frequency requires special care since it alters the fundamental period T. Nevertheless laser frequency is undoubtedly an important control parameter in experiments. Pulse chirping, for example, is considered to be a powerful tool for molecular dissociation control and/or quantum population control [53,54]. The apparent difficulty in its Floquet based formulation, however, was shown [55] to be circumvented by using the phase variable θ instead of periodic time variable s [55]. Here we apply this idea to derive the nonadiabatic time evolution equation including frequency variation in terms of two-time formalism. We use the phase variable θ instead of short-time variable s to define the extended Hamiltonian $\widetilde{H}_{t,\theta}$, which is periodic in θ in the sense $\widetilde{H}_{t,\theta} = \widetilde{H}_{t,\theta+2\pi}$. It reduces to the physical Hamiltonian at $\theta = \Theta(t)$, where $\Theta(t)$ is the physical phase as a function of t. The physical phase may be set as $\Theta(t) = \omega(t)t + \text{const}$, as Guerin assumed, but it may take other forms. We here introduce the instant (differential) frequency Ω_t to define $\Theta(t) = \int^t d\tau \Omega_\tau$. The Schrödinger equation for the extended state becomes

$$i\hbar\partial_t \widetilde{\Psi}_{t,\theta} = \mathcal{H}_{t,\theta}\widetilde{\Psi}_{t,\theta}, \tag{A1}$$

where $\mathcal{H}_{t,\theta} = H_{t,\theta} - i\hbar\Omega_t\partial_\theta$ is the Floquet Hamiltonian, which is formally periodic in θ. As we did in the main text, we assume that the t dependence can be absorbed in the parameter and rewrite the Floquet Hamiltonian as $\mathcal{H}_\theta(\mathcal{R}_t)$. The nonadiabatic time evolution equation reads

$$\begin{aligned} i\hbar\dot{\chi}_\alpha(\mathbf{R}) = &\sum_I \frac{1}{2M_I}\sum_\beta \left(\left[\frac{\hbar}{i}\frac{\partial}{\partial \mathbf{R}^I} - \frac{Q_I}{c}\mathbf{A} - i\hbar\mathbf{X}\right]^2\right)_{\alpha\beta}\chi_\beta \\ &+ U_{\text{nuc}}(\mathbf{R})\chi_\alpha + \lambda_\alpha\chi_\alpha - i\hbar\sum_\mu \dot{\zeta}^\mu \sum_\beta \mathcal{X}^{(\zeta^\mu)}_{\alpha\beta}\chi_\beta. \end{aligned} \tag{A2}$$

The formal appearance of Eq. (A2) is equivalent to that of Eq. (13), although the inner product is now defined as

$$\langle\langle\alpha|\beta\rangle\rangle \equiv \int \frac{d\theta}{2\pi}\langle\alpha(\theta)|\beta(\theta)\rangle, \tag{A3}$$

and the adiabatic parameter set $\{\zeta_t^\mu\}$ includes Ω_t, which accompanies corresponding nonadiabatic coupling $\mathcal{X}^{(\Omega)}_{\alpha\beta}$ given as

$$\mathcal{X}^{(\Omega)}_{\alpha\beta} = \langle\langle\Phi_\alpha;\mathcal{R}_t|\frac{\partial}{\partial\Omega}|\Phi_\beta;\mathcal{R}_t\rangle\rangle = \frac{\langle\langle\Phi_\alpha;\mathcal{R}_t|i\hbar\partial_\theta|\Phi_\beta;\mathcal{R}_t\rangle\rangle}{\lambda_\alpha - \lambda_\beta}. \tag{A4}$$

If the physical phase is given by $\Theta_t = \omega(t)t + \phi$ (ϕ is the time-independent phase) after Refs. [53–55], we have $\Omega_t = \dot{\omega}(t)t + \omega(t)$ and the resultant time evolution of the physical wave function $\widetilde{\Psi}_{t,\theta}|_{\theta=\Theta_t}$ is equivalent to Ref. [55].

APPENDIX B: DETAILS OF QUASICLASSICAL APPROXIMATION

Here we discuss the details of the quasiclassical approximation. We first discuss Eq. (16). In Ref. [39], it was shown that the best classical representation (within the stationary

phase approximation) of nuclear dynamics is Newtonian dynamics with nonclassical force, which is an expectation value of electronic operator $-\frac{\partial H^{el}}{\partial \mathbf{R}}$ along the time evolution of the system. Calculation of this special type of expectation value requires the knowledge of the time evolution of the electronic degrees of freedom, which, in the general case, leads to an extremely difficult self-consistency problem. In the region with negligible nonadiabatic transitions, however, the adiabatic state $|\Phi_\alpha(t);\mathcal{R}_t\rangle$, after a sufficiently short time, obviously evolves into the corresponding state on the nearby nuclear position. The effective force is hence given by the adiabatic state average. The argument here obviously extends to generalized nonadiabaticity, since it is the Floquet state which is (quasi)stationary under the laser field. The effective force is hence given by Eq. (16) in the main text.

We next derive an explicit estimate of small nonadiabaticity. Using a nondimensional estimate of nuclear derivative contribution, smallness of nonadiabaticity between two Floquet states $|\Phi_\alpha;\mathcal{R}_t\rangle$ and $|\Phi_\beta;\mathcal{R}_t\rangle$ with quasienergy λ_α and λ_β is given as

$$\frac{|i\hbar\mathbf{v}\cdot\mathbf{X}_{\alpha\beta}|}{|\lambda_\alpha-\lambda_\beta|}\ll 1, \tag{B1}$$

where $\mathbf{v}=\dot{\mathbf{R}}$ is the velocity of the nuclei in the sense of classical representation. Using the fact $\langle\!\langle\Phi_\alpha|\frac{\partial}{\partial\zeta}|\Phi_\beta\rangle\!\rangle = \langle\!\langle\Phi_\alpha|-\frac{\partial\mathcal{H}^{\rm ele}}{\partial\zeta}|\Phi_\beta\rangle\!\rangle/(\lambda_\alpha-\lambda_\beta)$, Eq. (B1) is rewritten as

$$\frac{\left|i\hbar\mathbf{v}\cdot\langle\!\langle\Phi_\alpha;\mathcal{R}_t|\left(-\frac{\partial\mathcal{H}^{\rm ele}}{\partial\mathbf{R}}\right)|\Phi_\beta;\mathcal{R}_t\rangle\!\rangle\right|}{(\lambda_\alpha-\lambda_\beta)^2}\ll 1. \tag{B2}$$

A similar estimate for the smallness of field-induced nonadiabaticity is given as, in the dipole gauge,

$$\frac{|i\hbar\dot{E}\boldsymbol{\varepsilon}\cdot\langle\!\langle\Phi_\alpha;\mathcal{R}_t|\boldsymbol{\mu}|\Phi_\beta;\mathcal{R}_t\rangle\!\rangle|}{(\lambda_\alpha-\lambda_\beta)^2}\ll 1, \tag{B3}$$

where $\boldsymbol{\varepsilon}$ is the field polarization vector, E and $\dot{E}$ are the electric-field amplitude and its time derivative (such as pulse envelope and its time derivative), and $\boldsymbol{\mu}$ is the dipole operator. The corresponding expression for the velocity gauge can also be obtained in an obvious manner.

It obviously follows that near avoided-crossing points that adiabaticity is broken for the range where the difference of two adjacent quasienergies is smaller than the energy scale given by the square root of the numerator appearing in the left-hand side of Eqs. (B2) or (B3).

APPENDIX C: APPROXIMATE DIABATIZATION OF MATRIX ELEMENTS

Here we show some details of the approximate diabatization scheme. We start from an $N_{\rm tot}$ dimensional adiabatic basis set and corresponding matrices. We first select a subset of adiabatic vectors $\{|F_a;\mathbf{R}\rangle\}_{a\in\Lambda}$ where Λ is a fixed subset of the adiabatic vector index set $\Lambda_0=[1,N_{\rm tot}]$. We first diagonalize the submatrix of the dipole matrix (parallel to the molecular axis) $D^{\parallel}_{ab}|_{a,b\in\Lambda}$ as

$$\sum_{b\in\Lambda}{}' D^{\parallel}_{ab}U^b_p=\mu_p U^a_p, \tag{C1}$$

where U^a_p denotes the ath component of pth eigenvector of the dipole submatrix and μ_p is the corresponding eigenvalue. The corresponding state is defined as $|U_p;\mathbf{R}\rangle\equiv\sum'_a|F_a;\mathbf{R}\rangle U^a_p$. The derivative couplings of these state vectors are evaluated as (the derivation will be given later)

$$\langle U_p;\mathbf{R}|\frac{\partial}{\partial\mathbf{R}}|U_q;\mathbf{R}\rangle = -\frac{\sum'_{b,a\in\Lambda}U^{b*}_p\sum_{r\notin\Lambda}(D^{\parallel}_{br}\mathbf{X}_{r,a}-\mathbf{X}_{b,r}D^{\parallel}_{ra})U^a_q}{\mu_p-\mu_q}, \tag{C2}$$

where $\sum'_{b,a\in\Lambda}$ indicates the summation over subset Λ, while $\sum_{r\notin\Lambda}$ indicates the summation over the residual set $\Lambda_0\setminus\Lambda$. For the actual calculation of LiF in the main text, the lowest two adiabatic states are thus transformed (i.e., $\Lambda=\{0,1\}$), to $|U_I;\mathbf{R}\rangle$ and $|U_C;\mathbf{R}\rangle$, which are essentially ionic and covalent, respectively. These two transformed state vectors as well as the lowest N_b-2 of remaining adiabatic vectors, $\{|U_I\rangle,|U_C\rangle,|F_3\rangle,\ldots,|F_{N_b}\rangle\}$ are used in the calculation of dynamics. The derivative coupling elements obtained in this transformation are shown in Fig. 3(d).

We now evaluate the nuclear coordinate derivatives of state vector $|U_p;\mathbf{R}\rangle$ defined as $\sum'_a|F_a\rangle U^a_p$ where the summation with prime ($\sum'$) is used to emphasize that the summation of indices runs over the restricted set Λ. The derivative couplings among state vectors $|U_p;\mathbf{R}\rangle$ are expanded as

$$\begin{aligned}\langle U_p;\mathbf{R}|\frac{\partial}{\partial\mathbf{R}}|U_q;\mathbf{R}\rangle &= \sum_a{}'\langle U_p;\mathbf{R}|F_a;\mathbf{R}\rangle\frac{\partial}{\partial\mathbf{R}}U^a_q \\ &\quad+\sum_a{}'\langle U_p;\mathbf{R}|\frac{\partial}{\partial\mathbf{R}}|F_a;\mathbf{R}\rangle U^a_q \\ &= \sum_a{}'U^{a*}_p\frac{\partial}{\partial\mathbf{R}}U^a_q+\sum_{b,a}{}'U^{b*}_p\mathbf{X}_{ba}U^a_q.\end{aligned} \tag{C3}$$

It follows from the fact that the coefficient vector U^a_q is the eigenvector of the matrix $D^{\parallel}_{ab}$ that

$$\sum_a{}'U^{a*}_p\frac{\partial}{\partial\mathbf{R}}U^a_q=-\frac{\sum_a{}'U^{a*}_p\frac{\partial}{\partial\mathbf{R}}(D^{\parallel}_{ab})U^b_q}{\mu_p-\mu_q}. \tag{C4}$$

Introducing the basis vector independent operator form of the dipole $\hat{D}^{\parallel}$, the derivative of the matrix element is evaluated as (using index i to emphasize unrestricted summation)

$$\frac{\partial}{\partial\mathbf{R}}(D^{\parallel}_{ab})=\frac{\partial}{\partial\mathbf{R}}\langle F_a|\hat{D}^{\parallel}|F_b\rangle=\sum_i(D^{\parallel}_{ai}\mathbf{X}_{i,b}-\mathbf{X}_{a,i}D^{\parallel}_{i,b}), \tag{C5}$$

where the dipole operator itself, being a purely electronic operator, is assumed to be independent of nuclear coordinates:

$\frac{\partial}{\partial \mathbf{R}}\hat{D}^{\parallel}=0$. We hence have

$$\begin{aligned}\langle U_p;\mathbf{R}|\frac{\partial}{\partial \mathbf{R}}|U_q;\mathbf{R}\rangle &= -\frac{\sum'_{b,a}U_p^{b*}\sum_i(D^{\parallel}_{bi}\mathbf{X}_{ia}-\mathbf{X}_{bi}D^{\parallel}_{ia})U_q^a}{\mu_p-\mu_q}\\ &\quad+\sum_{b,a}{}'U_p^{b*}\mathbf{X}_{ba}U_q^a\\ &= -\frac{\sum'_{b,a}U_p^{b*}\sum_{r\notin\Lambda}(D^{\parallel}_{br}\mathbf{X}_{r,a}-\mathbf{X}_{b,r}D^{\parallel}_{ra})U_q^a}{\mu_p-\mu_q},\end{aligned}\tag{C6}$$

which proves Eq. (C2).

APPENDIX D: EXACT DESCRIPTION OF NONADIABATIC TRANSITION

We show an exact expression of nonadiabatic transition moment taking into account of the extended nature of the nuclear wave function. We use Eq. (13) to derive the time derivative of the local Floquet state population $\rho_\alpha(\mathbf{R},t)\equiv|\chi_\alpha(\mathbf{R},t)|^2$. A straightforward calculation gives

$$\begin{aligned}\dot{\rho}_\alpha(\mathbf{R},t) &= -\sum_I\nabla_I\cdot\mathbf{J}^I_{\alpha\alpha}-\sum_{I,\beta}\frac{1}{2}\left[\mathbf{X}^I_{\alpha\beta}\cdot\mathcal{J}^I_{\alpha\beta}+\text{c.c.}\right]\\ &\quad+\sum_{I,\beta}\frac{1}{2}\left[\mathbf{X}^I_{\beta\alpha}\cdot\mathcal{J}^I_{\beta\alpha}+\text{c.c.}\right]\\ &\quad-2\sum_\mu\dot{\zeta}^\mu\text{Re}\left(\chi^*_\alpha(\mathbf{R},t)\chi_\beta(\mathbf{R},t)\mathcal{X}^{\zeta^\mu}_{\alpha\beta}\right),\end{aligned}\tag{D1}$$

where $\mathcal{J}^I_{\alpha\beta}$ denotes the "covariant" currentlike quantity related to the Ith nuclear coordinate defined as

$$\mathcal{J}^I_{\alpha\beta}\equiv\frac{1}{M_I}\sum_\gamma\chi^*_\alpha(\mathbf{R},t)\left[\left(\frac{\hbar}{i}\nabla-\frac{q}{c}\mathbf{A}\right)\delta_{\beta\gamma}-i\hbar\mathbf{X}^I_{\beta\gamma}\right]\chi_\gamma(\mathbf{R},t)\tag{D2}$$

and $\mathbf{J}^I_\alpha$ is the projected current,

$$\mathbf{J}^I_\alpha\equiv\tfrac{1}{2}\left(\mathcal{J}^I_{\alpha\alpha}+\text{c.c.}\right).\tag{D3}$$

The meaning of Eq. (D1) is now clear; the first term describes the drift contribution while the second and the third terms (each including c.c.) describe the transition induced by nuclear motion through the derivative coupling. The fourth term is the contribution from the time-dependent change of the laser parameters. Mixed quantum classical description, or the narrow wave-packet limit, would give

$$\begin{aligned}\frac{d}{dt}|C_\alpha|^2 &= -\sum_I\mathbf{v}^I\cdot\left(C^*_\alpha\mathbf{X}^I_{\alpha\beta}C_\beta+\text{c.c.}\right)\\ &\quad-2\sum_\mu\dot{\zeta}\,Re\left(C^*_\alpha X^{\zeta^\mu}_{\alpha\beta}C_\beta\right),\end{aligned}\tag{D4}$$

where C_α denotes the coefficient of Floquet state α, and $\mathbf{v}^I$ is the Ith nuclear velocity (in the sense of mixed quantum classical representation). The first term in Eq. (D4) corresponds to the second and third terms in Eq. (D1), while the second term in Eq. (D4) corresponds to the fourth term.

[1] B. J. Sussman, D. Townsend, M. Yu. Ivanov, and A. Stolow, Science **314**, 278 (2006).
[2] O. Smirnova, Y. Mairesse, S. Patchkovskii, N. Dudovich, D. Villeneuve, P. Corkum, and M. Y. Ivanov, Nature (London) **460**, 972 (2009).
[3] A. E. Boguslavskiy, J. Mikosch, A. Gijsbertsen, M. Spanner, S. Patchkovskii, N. Gador, M. J. J. Vrakking, and A. Stolow, Science **335**, 1336 (2012).
[4] M. Protopapas, C. H. Keitel, and P. L. Knight, Rep. Prog. Phys. **60**, 389 (1997).
[5] M. F. Kling and M. J. Vrakking, Annu. Rev. Chem. Phys. **59**, 463 (2008).
[6] F. Krausz and M. Y. Ivanov, Rev. Mod. Phys. **81**, 163 (2009).
[7] S. Shi and H. Rabitz, J. Chem. Phys. **92**, 364 (1990); R. S. Judson and H. Rabitz, Phys. Rev. Lett. **68**, 1500 (1992); R. Levis, G. Menkir, and H. Rabitz, Science **292**, 709 (2001).
[8] G. Sansone, F. Kelkensberg, J. F. Perez-Torres, F. Morales, M. F. Kling, W. Siu, O. Ghafur, P. Johnsson, M. Swoboda, E. Benedetti, F. Ferrari, F. Lepine, J. L. Sanz-Vicario, S. Zherebtsov, I. Znakovskaya, A. L'Huillier, M. Y. Ivanov, M. Nisoli, F. Martin, and M. J. J. Vrakking, Nature (London) **465**, 763 (2010).
[9] H. J. Wörner, J. B. Bertrand, D. V. Kartashov, P. B. Corkum, and D. M. Villeneuve, Nature (London) **466**, 604 (2010).
[10] D. Shafir, H. Soifer, B. D. Bruner, M. Dagan, Y. Mairesse, S. Patchkovskii, M. Y. Ivanov, O. Smirnova, and N. Dudovich, Nature (London) **485**, 343 (2012).
[11] E. Runge and E. K. U. Gross, Phys. Rev. Lett. **52**, 997 (1984).
[12] Shih-I. Chu, J. Chem. Phys. **123**, 062207 (2005).
[13] S.-K. Son and Shih-I. Chu, Phys. Rev. A **80**, 011403(R) (2009).
[14] T. Kato and H. Kono, Chem. Phys. Lett. **392**, 533 (2004).
[15] J. Colgan, M. S. Pindzola, and F. Robicheaux, J. Phys. B **37**, L377 (2004).
[16] S. Chelkowski, A. Conjusteau, T. Zuo, and A. D. Bandrauk, Phys. Rev. A **54**, 3235 (1996).
[17] I. Kawata, H. Kono, and Y. Fujimura, J. Chem. Phys. **110**, 11152 (1999).
[18] M. Born and R. Oppenheimer, Ann. Phys. **84**, 457 (1927).
[19] J. M. Browman and G. C. Schatz, Annu. Rev. Phys. Chem. **46**, 139 (1995).
[20] L. J. Butler, Annu. Rev. Phys. Chem. **49**, 125 (1998).
[21] A. W. Jasper, C. Zhu, S. Nangia, and D. G. Truhlar, Faraday Discuss. **127**, 1 (2004).
[22] K. Takatsuka, Int. J. Quantum Chem. **109**, 2131 (2009).
[23] J. Shirley, Phys. Rev. **138**, B979 (1965).
[24] Shih-I. Chu and D. A. Telnov, Phys. Rep. **390**, 1 (2004).
[25] G. Floquet, Ann. l'Ecol. Norm. Suppl. **12**, 47 (1883).
[26] S. H. Autler and C. H. Townes, Phys. Rev. **100**, 703 (1955).
[27] A. Bandrauk and M. Sink, Chem. Phys. Lett. **57**, 569 (1978).

[28] L. J. Frasinski, J. H. Posthumus, J. Plumridge, K. Codling, P. F. Taday, and A. J. Langley, Phys. Rev. Lett. **83**, 3625 (1999).
[29] A. Zavriyev, P. H. Bucksbaum, J. Squier, and F. Saline, Phys. Rev. Lett. **70**, 1077 (1993).
[30] A. Giusti-Suzor, X. He, O. Atabek, and F. H. Mies, Phys. Rev. Lett. **64**, 515 (1990).
[31] A. Zavriyev, P. H. Bucksbaum, H. G. Muller, and D. W. Schumacher, Phys. Rev. A **42**, 5500 (1990).
[32] Shih-I. Chu, J. Chem. Phys. **94**, 7901 (1991).
[33] G. Yao and Shih-I. Chu, Chem. Phys. Lett. **197**, 413 (1992).
[34] T. Ho and Shih-I. Chu, Chem. Phys. Lett. **141**, 315 (1987); see also related discussions in Ref. [24].
[35] U. Peskin and N. Moiseyev, J. Chem. Phys. **99**, 4590 (1993).
[36] M. Chrysos, O. Atabek, and R. Lefebvre, Phys. Rev. A **48**, 3845 (1993).
[37] R. Lefebvre, O. Atabek, M. Šindelka, and N. Moiseyev, Phys. Rev. Lett. **103**, 123003 (2009).
[38] Advanced numerical calculations of multidimensional nonadiabatic dynamics based on the mixed quantum classical representation are found in, for example, (1) M. Amano and K. Takatsuka, J. Chem. Phys. **122**, 084113 (2005); and (2) K. Nagashima and K. Takatsuka, J. Phys. Chem. A **113**, 15240 (2009); the subject was recently reviewed in (3) T. Yonehara, K. Hanasaki, and K. Takatsuka, Chem. Rev. **112**, 499 (2011).
[39] K. Hanasaki and K. Takatsuka, Phys. Rev. A **81**, 052514 (2010); the essential ideas were established in P. Pechukas, Phys. Rev. **181**, 166 (1969).
[40] A number of advanced calculation methods in nonadiabatic chemical dynamics are reviewed in Ref. [38] (3), although the validity of the Floquet formalism is yet to be tested.
[41] F. Bunkin and I. Tugov, Phys. Rev. A **8**, 601 (1973).
[42] D. Kosloff and R. Kosloff, J. Comput. Phys. **52**, 35 (1983).
[43] A. Giusti-Suzor, F. H. Mies, L. F. DiMauro, E. Charron, and B. Yang, J. Phys. B **28**, 309 (1995).
[44] G. N. Gibson, M. Li, C. Guo, and J. Neira, Phys. Rev. Lett. **79**, 2022 (1997).
[45] L. Kahn, P. Hay, and I. Shavitt, J. Chem. Phys. **61**, 3530 (1974).
[46] A. Varandas, J. Chem. Phys. **131**, 124128 (2009).
[47] A. Bandrauk and J. Gauthier, J. Phys. Chem. **93**, 7552 (1989).
[48] K. Yagi and K. Takatsuka, J. Chem. Phys. **123**, 224103 (2005).
[49] M. Schmidt, K. Baldridge, J. Boatz, S. Elbert, M. Gordon, J. Jensen, S. Koseki, N. Matsunaga, K. Nguyen, S. Su, T. Windus, M. Dupuis, and J. Montgomery, J. Comput. Chem. **14**, 1347 (1993).
[50] J. Paldus, Phys. Rev. A **14**, 1620 (1976); I. Shavitt, Int. J. Quantum Chem. **12**(S11), 131 (1977).
[51] The nonadiabatic coupling matrices in the adiabatic representation are obtained using the formula $\mathbf{X}_{\alpha\beta} = \frac{\langle\alpha|\frac{\partial H^{\mathrm{ele}}}{\partial \mathbf{R}}|\beta\rangle}{\mathcal{E}_\beta - \mathcal{E}_\alpha}$, where $|\alpha\rangle$ and $\mathcal{E}_\alpha$ are the αth adiabatic state and its energy, respectively. The matrices required in this formula are transformed from the CSF representation that are obtained using analytic derivatives in the way detailed in Ref. [38] (1).
[52] R. Kendall, T. Dunning, and R. Harrison, J. Chem. Phys. **96**, 6796 (1992); T. Dunning, *ibid.* **90**, 1007 (1989).
[53] S. Chelkowski, A. D. Bandrauk, and P. B. Corkum, Phys. Rev. Lett. **65**, 2355 (1990).
[54] S. Zhdanovich, E. A. Shapiro, M. Shapiro, J. W. Hepburn, and V. Milner, Phys. Rev. Lett. **100**, 103004 (2008).
[55] S. Guerin, Phys. Rev. A **56**, 1458 (1997).